Band-Tail Model and Temperature-Induced Blue-Shift in Photoluminescence Spectra of $In_xGa_{1-x}N$ Grown on Sapphire

PETR G. ELISEEV,[1,3] MAREK OSINSKI,[1] JINHYUN LEE,[1] TOMOYA SUGAHARA,[2] and SHIRO SAKAI[2]

1.—University of New Mexico, Center for High Technology Materials, 1313 Goddard SE, Albuquerque, NM 87106. 2.—University of Tokushima, Department of Electrical and Electronic Engineering, 2-1 Minami-josanjima, Tokushima, Japan. 3.—Also with P.N. Lebedev Physics Institute, Russian Academy of Sciences, Moscow, Russia

A band-tail model of inhomogeneously broadened radiative recombination is presented and applied to interpret experimental data on photoluminescence of various bulk and quantum-well epitaxial InGaN/GaN structures grown by MOCVD. The temperature dependence of the spectral peak position is analyzed according to the model, explaining the anomalous temperature-induced blue spectral shift. Significant differences are observed between epilayers grown on sapphire substrates and on GaN substrates prepared by the sublimation method. No apparent evidence of band tails in homoepitaxial structures indicates their higher crystalline quality.

Key words: Wide-bandgap semiconductors, InGaN, photoluminescence, band tails, homoepitaxy

INTRODUCTION

The ternary alloy $In_xGa_{1-x}N$ has become a very important material in semiconductor physics. It can be fabricated as a thin film in different multilayer group-III nitride structures, and in spite of its poor crystalline quality it serves as efficient luminescent material in UV and visible light-emitting diodes and diode lasers.[1–4] It also seems promising for high-temperature optoelectronics, since its radiative quantum yield does not drop significantly as the ambient temperature is increased from 300 to 450 K.[5]

Even though InGaN-based devices have reached commercial maturity, the radiative emission processes in this material are not yet well understood. According to Ref. 6, emission in InGaN can be assigned to recombination of excitons localized at potential energy minima in the quantum well. From a study of multiple quantum wells, it was concluded that the exciton localization occurs at deep traps, which could be originated from indium-rich regions acting as quantum dots.[7] Some spectral features of InGaN-containing structures are rather unusual. As the ambient temperature increases, the emission peak undergoes an anomalous blue shift.[8–11] In addition, it was found that the emission peak spans continuously a wide spectral range (~0.2 eV) when the current ranges over ~6 decades.[8] A strong contribution of non-thermal broadening is characteristic of the electroluminescence spectra of AlGaN/InGaN/GaN single quantum wells.[9,10] A likely involvement of band-tail states was also pointed out.[9–13]

There are several issues with the InGaN alloy concerning its physical-chemical properties and fabrication methods. These are crystalline quality of hetero- and homoepitaxial material, residual stress/strain and piezoelectric fields, and alloy stability. All of these factors seem to influence the radiative recombination processes. In this paper, we present in detail a simple analytical model of recombination involving band-tail states that can be caused by a strong variation of the energy bandgap due to statistical fluctuations of alloy composition and, possibly, to correlated variations of composition that may be caused by technological factors or by instability associated with phase separation. The model is then applied to InGaN and compared with results of extensive spectral studies of photoluminescence from different InGaN-based epitaxial materials: bulk layers, single quantum wells, and multiple-quantum-well structures. We interpret the efficient radiative process in InGaN to be the result of fast capture of excess carriers into the band-tail states, with a subsequent radiative recombination. We focus on the temperature dependence of the spec-

(Received September 20, 1999; accepted December 20, 1999)

tral peak position, which allows us to describe different types of behavior in terms of the band-tail model and to derive the energy parameter of tails describing the inhomogeneous broadening of the band edges.

THE BAND-TAIL MODEL

General Remarks

Band tails can appear in the electron energy spectrum of solids as a result of disordering in the crystalline structure introduced by defects, impurities and non-uniformity of chemical composition. The best known examples of such tails are in amorphous and heavily doped semiconductors (see, e.g., Ref. 14). Application of the band-tail concept to heavily-doped light-emitting diodes and diode lasers had been considered in Ref. 15, where occupation of the Gaussian density-of-states (DOS) tails was analyzed.

In a heavily doped semiconductor, disordering is associated with the random Coulomb fields of ionized impurities. In InGaN, the nature of band-tail states is different; they appear even in undoped material, due to strong compositional non-uniformity. We emphasize that composition-related tail states are suitable to provide efficient luminescence because, as opposed to ionized impurities, these states attract both types of carriers: potential wells for both electrons and holes are associated with the same site (indium-rich cluster). Due to this, the matrix element for optical transitions can be as large as in the case of free carriers. In heavily doped semiconductors, the random electric potential of the Coulomb centers produces distant extremes of band edges that separate carriers of opposite sign. This leads to an increase in the lifetime of carriers captured into deep tail states, due to a reduced matrix element.

Another particular feature of tail states in InGaN is that the composition variations are not only caused by statistical fluctuations, but may result from partial decay of the alloy, associated with its thermodynamic instability.[16] This can produce more significant broadening of band edges than in heavily doped semiconductors.

In light-emitting structures, the tail states are very important, because they provide the lowest-energy levels available for the carriers. Consequently, these states are occupied by excess minority carriers (or by both kinds of carriers) starting from very low pumping rates. Also, these states are the first ones to reach inverted population in lasers under higher pumping rate. The occupation of tails is more sensitive to the pumping rate than the occupation in regular energy bands, because the DOS in tails is much lower. This produces strong band-filling effects characteristic of band tails (blue shift of the emission peak with an increasing pumping rate). On the other hand, the tails are a result of excessive inhomogeneous broadening in the system, and its contribution to spectral bandwidth leads to broader spontaneous emission spectra and higher lasing threshold.

We consider the language of band tails to be adequate for quantitative analysis of broad emission from InGaN. This is not in contradiction with a concept of localized excitons, which is more fruitful for very narrow linewidth emission in many semiconductors, including GaN. As an electron-hole pair is captured into tail states, the state occupation can be described as that of fermions, with Fermi-Dirac statistics. This is an important tool for analysis that distinguishes localized excitons from the usual Bose-Einstein excitonic statistics.

Here we deal with certain DOS distribution in the band tails, without regard to what is the predominant cause of the energy level spreading. In agreement with the traditional approach, we assume that multiple factors can lead to the Gaussian statistics of the spreading. These factors are: 1) a real shape of profiles for potential energy in cluster-related wells, 2) the Coulomb interaction of localized carriers, 3) free-carrier screening and other many-body effects, 4) exchange effects with neighboring clusters, 5) piezoelectric effects due to residual lattice strain, 6) pyroelectric effects due to spontaneous dielectric polarization. We believe that resulting DOS distribution is sufficiently stable in order to apply the regular distribution functions for occupation probability of tail states. If this approach were not producing satisfactory results, specific corrections would have to be introduced, for example, accounting for many-body effects.

DOS Distribution

The local band edge (1e, 1hh levels for quantum wells, conduction- and valence-band edges for bulk material) is assumed to fluctuate due to compositional variations. The average density of states (DOS) as a function of energy should be calculated as[14]

$$\rho(E) = \int \rho(E,V)\, P(V)\, dV \qquad (1)$$

where $\rho(E,V)$ is the local DOS function, $P(V)$ is the probability distribution, and V is the local band-edge energy. The averaging procedure leads to smoothening of the sharp edge of the DOS distribution. Let us assume that the two-dimensional DOS in quantum wells has a step-like shape:

$$\rho(E,V) = (m^*/\pi\hbar^2)\sum_i \vartheta(E - V_i) \qquad (2)$$

where m^* is the effective mass, ϑ is the Heaviside step function [$\vartheta(x) = 1$ for $x > 0$ and $\vartheta(x) = 0$ for $x < 0$], and i is the subband index. We consider the shape modification of the lowest subband edge, $i = 1$. The probability function is assumed to be Gaussian:

$$P(V) = (2^{1/2}\pi^{1/2}\sigma)^{-1} \exp\,[-(V - V_0)^2/(2\sigma^2)] \qquad (3)$$

where σ is the energy parameter of the distribution, and V_0 is the central position of the local band edge (the nominal band edge). The averaging procedure as in Eq. 1 gives

$$\rho(E) = (m^*/2\pi\hbar^2)\{1 + \mathrm{erf}\,[(E - V_0)/(2^{1/2}s)]\} \qquad (4)$$

This expression predicts the DOS to be twice lower at

the nominal edge $E = V_0$ than before averaging, and to decrease in the tail below the nominal edge. The asymptotic behavior of $\rho(E)$ (at energies deep inside the nominal bandgap) corresponds to a Gaussian.

The parameter σ describes the broadening effect and the shape of the tail. In this simple approach, it is the only adjustable parameter. In general, this corresponds to the assumption of a distribution with non-vanishing moments only up to the second order. If higher-order moments are substantial, the distribution can be more complicated (asymmetric, etc.).

Under some circumstances, these assumptions can be modified. One case is correlation in the compositional clusters (due to phase separation or chemical reordering). For example, phase separation caused by annealing can lead to formation of indium-rich clusters of ultimate phase composition. If this process is completed, there will be a predominance of clusters with a definite composition. The random factor would be the size of clusters, but not their composition. There would be no states deeper than some specific level, corresponding to the ultimate phase composition. Thus, the asymptotic part of the DOS distribution would deviate from the Gaussian shape.

Band-Tail Model: Carrier Occupation of Gaussian Band Tails

The model of quasi-equilibrium occupation with a Gaussian DOS was proposed earlier for heavily doped GaAs diode lasers.[15] Under an increasing pumping rate, two types of behavior can in principle be observed in luminescence spectra: 1) a stable peak position, corresponding to non-degenerate occupation; and 2) a blue-shifting peak corresponding to degenerate occupation (band-filling). Both behaviors can be illustrated by a simple example of carrier distribution N(E) in the energy scale of one of the tails, as shown in Fig. 1a for a range of Fermi-level positions in a quantum well. The DOS distribution corresponding to Eq. 4 is marked with a thick line. This distribution has a Gaussian asymptote deep inside the bandgap, but differs from the Gaussian function near the nominal (not-broadened) band edge E_0. Thin lines in Fig. 1a represent the carrier distributions with their maxima marked by dots. At low pumping rates, when the normalized Fermi level $(F - E_0)/\sigma < -3$, the peak of the carrier distribution has a stable position with a constant bandwidth. At higher pumping rates, the peak is pulled by the Fermi level towards the high-energy side. The non-degenerate occupation is typical for lower pumping rates and higher temperatures, while the degenerate occupation is typical for higher pumping rates and lower temperatures. An interesting feature of the redistribution of carriers with increasing temperature is shown in Fig. 1b. As temperature rises, the peak of the curves moves towards higher energy. This effect is similar to ionization of local levels, but extended to the case of a continuous energy spectrum. This shift can lead to a blue temperature-induced shift of the emission peak, when the rate of the shift overcomes the rate of the temperature-induced bandgap shrinkage.

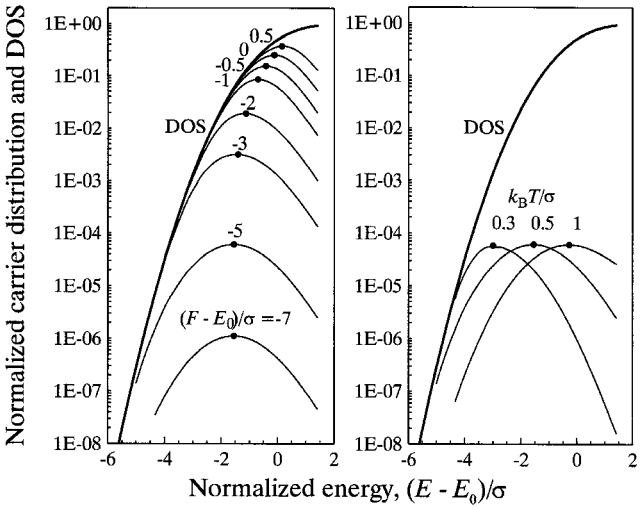

Fig. 1. Calculated normalized DOS distribution (thick lines) and carrier distributions (thin lines), both in units of $m^*/2\pi\hbar^2$, in function of the normalized energy $(E - E_0)/\sigma$, where E_0 is the nominal confined energy level in the quantum well . Dots mark the peak position. (a) Evolution of carrier distribution with increasing normalized Fermi energy $(F - E_0)/\sigma$ at constant temperature $T = \sigma/2k_B$. (b) Evolution of carrier distribution with temperature rise at approximately constant carrier density (normalized temperature is given in units of σ/k_B, where k_B is Boltzmann's constant).

Using the fact that the asymptotic behavior of $\rho(E)$ as given in Eq. (4) corresponds to a Gaussian, we make the following approximation for the DOS function $\rho_{e,h}(E)$ in the conduction and valence bands, respectively:

$$\rho_{e,h}(E) = \rho_{0e,h}\exp[-(E - E_{0e,h})^2/2\sigma_{e,h}^2] \qquad (5)$$

where ρ_{0e}, ρ_{0h}, E_{0e}, E_{0h}, σ_e, and σ_h are fixed parameters for band tails of electron and hole states. In particular, σ_e^2 and σ_h^2 are the dispersions of each Gaussian, E_{0e} is the center of the DOS Gaussian for the conduction band tail, and E_{0h} is the center of the DOS Gaussian for the valence band tail. Using Eq. 5, we can obtain analytical expressions for spontaneous emission spectra from non-degenerate band tails in a quantum well.

The optical transitions between the states of two tails are assumed to occur with no momentum conservation; hence the spectrum of spontaneous emission rate $r_{sp}(h\nu)$ can be represented by the integral convolution as follows:

$$r_{sp}(h\nu) = B(h\nu) \int \rho_e(E + h\nu)\, f_e(E + h\nu)\, \rho_h(E)\, f_h(E)dE \qquad (6)$$

where $f_e(E + h\nu)$ and $f_h(E)$ are the occupation functions for both involved tails, respectively, h is the Planck constant, ν is the photon frequency, and $B(h\nu)$ is the recombination coefficient. We also assume that both occupation functions are Fermi-Dirac distributions with a separate quasi-Fermi level F_e, F_h for each tail (the quasi-equilibrium approximation). In this consideration, we shall neglect the spectral dependence of $B(h\nu)$.

We focus on the behavior of the spectral peak $h\nu_p$ of the emission band. In the low-current case, we can assume $h\nu_p - \Delta F > k_BT$, where $\Delta F = F_e - F_h$ is the quasi-Fermi-level separation and k_B is the Boltzmann constant. This condition corresponds to non-degenerate occupation. Therefore, the Boltzmann tails of the occupation function can be used:

$$f_e(E,T,F_e) \cong \exp[(F_e - E)/k_BT] \quad (7a)$$

$$f_h(E,T,F_h) \cong \exp[(E - F_h)/k_BT] \quad (7b)$$

The carrier distributions N(E), P(E) for electrons and holes, respectively, can be calculated as follows:

$$N(E) = \rho_e(E)\, f_e(E,T,F_e)$$
$$= \rho_{0e} \exp[(F_e - E_{0e}^*)/k_BT] \exp(-\sigma_e^2/2k_B^2T^2)$$
$$\exp[-(E - E_{0e}^*)^2/2\sigma_e^2] \quad (8a)$$

$$P(E) = \rho_h(E)\, f_h(E,T,F_h)$$
$$= \rho_{0h} \exp[(E_{0h}^* - F_h)/k_BT] \exp(-\sigma_h^2/2k_B^2T^2)$$
$$\exp[-(E - E_{0h}^*)^2/2\sigma_h^2] \quad (8b)$$

where

$$E_{0e}^* = E_{0e} - \sigma_e^2/k_BT \quad (9a)$$

$$E_{0h}^* = E_{0h} + \sigma_h^2/k_BT \quad (9b)$$

As shown in Eq. 8, both carrier distributions over the energy scale are Gaussian with the same values of dispersion as in the corresponding DOS functions. The convolution of two Gaussians as specified in Eq. 6 gives again a Gaussian with the sum of partial dispersions:

$$r_{sp}(h\nu) = B \int N(E + h\nu)\, P(E)\, dE$$
$$= B^* \rho_{0e}\, \rho_{0h} \int \exp[-(E + h\nu - E_{0e}^*)^2/2\sigma_e^2]$$
$$\exp[-(E - E_{0h}^*)^2/2\sigma_h^2]\, dE$$
$$= B^* \rho_{0e}\, \rho_{0h} \exp[-(h\nu - h\nu_0)^2/2\sigma^2] \quad (10)$$

where

$$B^* = B \exp[-(\sigma_e^2 + \sigma_h^2)/2k_B^2T^2]$$
$$\exp[(\Delta F - h\nu_0)/k_BT] \quad (11a)$$

$$h\nu_0 = E_{0e}^* - E_{0h}^* \quad (11b)$$

$$\sigma^2 = \sigma_e^2 + \sigma_h^2 \quad (11c)$$

For a more general case, some non-Gaussian DOS distributions could be considered. Requirements for possible Gaussian-like distributions are: 1) reasonable asymptotic behavior deeply in the nominally forbidden band, 2) monotonic increase of the DOS from deep states to the nominal band edge, 3) smooth fitting to the undisturbed DOS somewhere near or above the nominal band edge.

A general rule for the position of the occupation maximum in a non-degenerate case for a monotonic DOS distribution is as follows:[15]

$$d\ln\rho/dE\,|_{peak} = (k_BT)^{-1} \quad (12)$$

This position is rather stable with the increasing pumping range until degeneracy occurs (cf. Fig. 1a). This means that the spontaneous emission peak is expected to be stable in the entire range of non-degenerate occupation (no band-filling effect). Therefore, any changes of the spectral position of the emission peak should be tested carefully with respect to: 1) occurrence of degeneracy with a transition to the usual band-filling effect, where the peak position is pulled by the quasi-Fermi levels; 2) change of DOS distribution by many-body effects; 3) total change of the dominant emission mechanism.

Temperature-Induced Shift of the Peak

Using Eq. 10, we can find that the spontaneous emission spectrum has a temperature-dependent peak at the photon energy

$$h\nu_0 = E_{0e}^* - E_{0h}^* = E_{0e} - \sigma_e^2/k_BT -$$
$$E_{0h} - \sigma_h^2/k_BT = E_0 - \sigma^2/k_BT \quad (13)$$

where $E_0 = E_{e0} - E_{h0}$ is the energy separation between the centers of Gaussian DOS distributions for electrons and holes, and σ^2/k_BT is the "red" shift of the emission peak relative to the energy distance between the Gaussian centers. The energy E_0 is close to the bandgap energy E_g, therefore, it can be assumed to depend on temperature in the same manner as E_g, namely,

$$E_0(T) = E_0(0) - \alpha T^2/(\beta + T) \quad (14)$$

where α and β are expected to be close to the usual Varshni parameters. We use Eqs. 13 and 14 to obtain curves of $(h\nu_0 - E_0)$ plotted in Fig. 2 as function of temperature. The upper thick curve illustrates the temperature dependence of E_0, obtained with $\alpha = 1$ meV/K, $\beta = 1196$ K for the Varshni parameters. These values have been extracted from photoreflectance measurements[17] of $In_{0.14}Ga_{0.86}N$ samples rather than from photoluminescence (PL) spectra. It was noticed in Ref. 17 that the PL peak was significantly red-

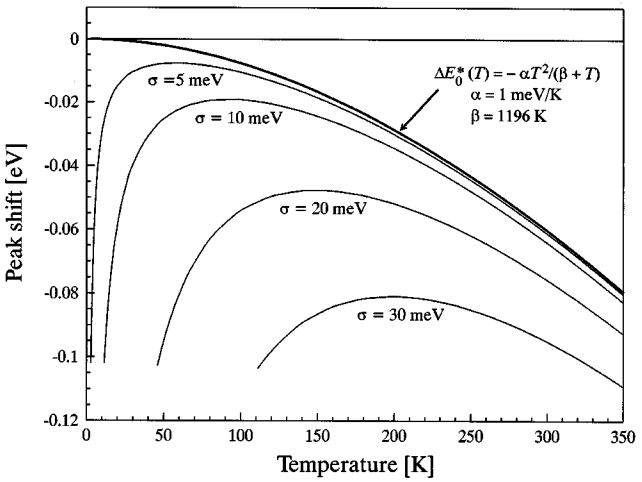

Fig. 2. Calculated peak position shift in function of temperature for a non-degenerate occupation of tail states. Thick curve corresponds to $\sigma = 0$ (no tails) and is given in the Varshni approximation. Thin curves correspond to various values of σ.

shifted compared to the actual bandgap energy. We emphasize here that band-tailing effects influence PL spectra much more strongly than photoreflectance spectra. The calculated curves in Fig. 2 illustrate this effect. The peak position follows the thin lines corresponding to various values of the tail parameter σ. The curves for spectral peak position are valid for the case of non-degenerate occupation. At very low temperatures, the dramatic decrease of the peak energy shown in Fig. 2 would actually be compensated due to degenerate occupation. In practice, degenerate occupation can be easily identified by observation of the emission peak shift with increasing pumping (due to the band-filling process). This type of peak position behavior has been clearly observed in electroluminescence studies of InGaN/ AlGaN/GaN quantum-well light-emitting diodes (LEDs).[9–11,18,19]

Within the framework of the band-tail model, the temperature-induced shift of the low-current spectral peak position $h\nu_0$ is as follows:

$$d(h\nu_0)/dT = dE_0/dT - d[(\sigma_e^2 + \sigma_h^2)/k_BT\,]/dT$$
$$= dE_g/dT + \sigma^2/k_BT^2 \qquad (15)$$

The sign of the temperature-induced shift is determined by dominant term on the right hand side of Eq. 15, with the negative bandgap term, and the positive band-tail term.

EXPERIMENTAL

Epitaxial layers and multilayer structures used in this work have been grown at the University of Tokushima by horizontal atmospheric-pressure MOCVD epitaxy. TMG (trimethylgallium), TMI (trimethylindium) and NH_3 were used as source gases. A thin GaN buffer layer was grown at 500°C, and then a GaN layer was grown at 1050°C.

Two types of substrates have been used: 1) sapphire, c-plane (0001), 2) "bulk" (needle-shaped) GaN $(10\bar{1}0)$, c- and m-plane, grown by sublimation method.[20] Single-heterostructure (SH) samples had an uncapped "bulk"-type InGaN layer grown at 800°C on a 2-μm-thick GaN buffer/substrate. The InGaN layer thickness ranged from 50 nm to 110 nm. Two other types of samples are single- and multiple-quantum-well (SQW and MQW) structures with InGaN wells and GaN barriers, sandwiched by GaN layers. Maximum cumulative InGaN thickness was in MQW samples was 20 nm, minimum (in SQW samples) was 0.8 nm. The average composition of alloys was in the range of 5-25% and had been controlled by the growth process. The average indium content was determined using x-ray diffraction measurements. All samples prepared for PL characterization were undoped. Data on structural analysis of such epitaxial structures were reported earlier.[21–24] For a single GaN layer, the transition of the film structure from grains with relatively independent orientation at about 300 nm to a uniform film with mosaic structure at 1.4 μm was observed. The threading dislocation density in epilayers ranges from 10^8 to 10^9 cm^{-2} in sapphire-substrate samples and is less than 10^6 cm^{-2} in homoepitaxial samples.

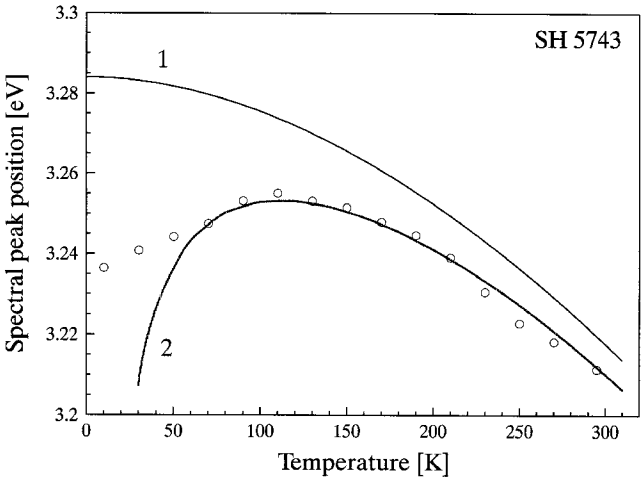

Fig. 3. PL peak position (circles) in function of temperature in a 110-nm-thick InGaN epilayer (single-heterostructure) No. 5743 emitting in the UV range. Curve 1 represents the nominal bandgap, curve 2 is for a non-degenerate occupation of band-tail states. Fitting parameters are $E_0(0) = 3.284$ eV, $\sigma = 14$ meV, $\alpha = 1.1$ meV/K. The value of β was fixed at 1196 K after Ref. 17.

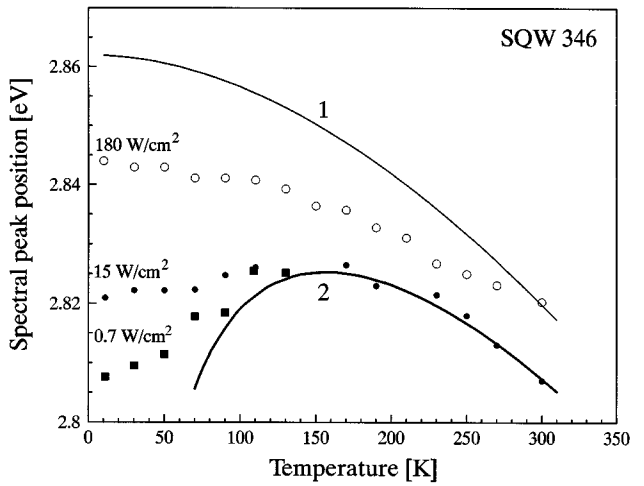

Fig. 4. PL peak position in function of temperature in GaN/InGaN/GaN SQW sample (thickness of InGaN layer is 1.4 nm) emitting in blue range (circles). Experimental points are for different pumping intensities at 325 nm, as indicated. Curve 1 is for a nominal band-gap variation with $E_0(0) = 2.862$ eV, $\alpha = 0.7$ meV/K, and $\beta = 1196$ K. Curve 2 is for a non-degenerate occupation of tail states with $\sigma = 18$ meV.

In PL measurements, a 325-nm UV line from He-Cd laser was used for surface pumping and a blue line at 442 nm was used for selective pumping of InGaN layers covered by GaN. The illuminated spot was about 50 μm in diameter. The incident optical power density was up to 180 W/cm². Measurements were performed using a closed-circuit refrigerator CTI-Cryogenics, model 22, to keep a sample at a fixed temperature. Spectra were recorded using a CVI double-grating spectrometer, model DK 242D, with a cooled GaAs-photocathode photomultiplier.

RESULTS OF MEASUREMENTS

In the course of PL measurements, we have observed several types of behavior of the InGaN spectral

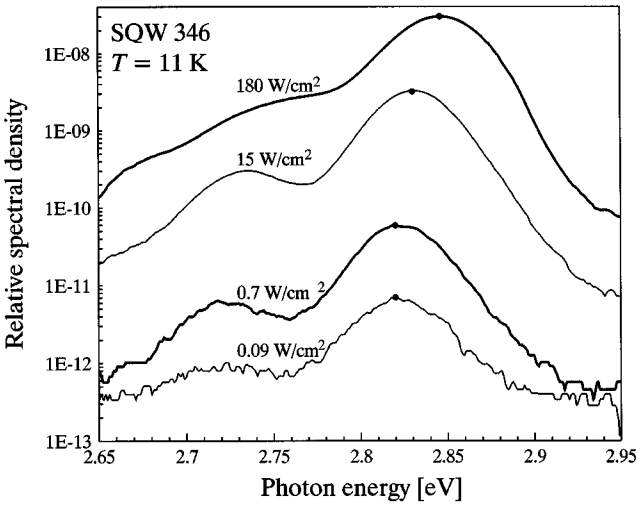

Fig. 5. PL spectra of the same GaN/InGaN/GaN SQW sample as in Fig. 4, taken at 11 K with varying pumping intensity controlled by calibrated neutral density filters. Peak position is marked by dots. The behavior of the main peak can be compared with curves in Fig. 1a.

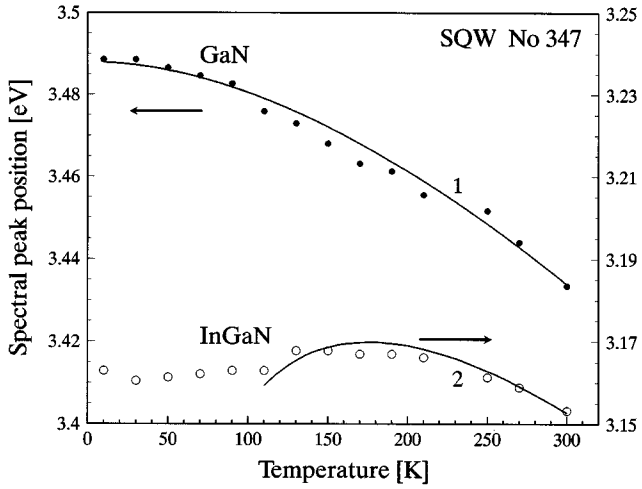

Fig. 6. PL peak position in function of temperature in GaN/InGaN/GaN 0.8-nm-thick SQW emitting in UV range for both GaN barrier emission (dots, left scale) and InGaN well emission (circles, right scale). Different types of behavior are identified with partial fitting by calculated curves 1 and 2 (see text).

peak. The main differences have been found between structures grown on sapphire and on bulk GaN substrates. In addition, even though the same PL pumping rate was maintained in all experiments, the actual excitation level could vary substantially from sample to sample, due to sample-dependent pumping efficiency (carrier collection into the InGaN layer) and variable nonradiative recombination rate. The first type of behavior is a non-monotonic temperature dependence as shown in Fig. 3 for the case of a SH InGaN structure with a 110-nm thick "bulk-type" InGaN layer. Experimental points show a continuous blue shift by ~20 meV when the temperature rises from 10 K to 110 K. At higher temperatures, in the range from 70 K to 300 K, the experimental points follow closely curve 2, calculated using Eqs. 13 and 14 with the tail parameter σ = 14 meV. This type of behavior includes a low-temperature part, where experimental points are above the "non-degenerate" curve 2, obviously because of some degeneracy, a middle-temperature part with an anomalous blue shift and a maximum photon energy (3.254 eV at 110 K in Fig. 3), and a high-temperature part with decreasing photon energy (110-300 K in Fig. 3).

Figure 4 presents the first type of peak behavior at a low pumping rate of 0.7 W/cm^2 (full squares) and another, second type of behavior at a high pumping rate of 180 W/cm^2. In the latter case (circles) the peak energy decreases in a monotonic manner from low temperature to room temperature by about 24 meV. However, this red shift is smaller than the corresponding bandgap temperature dependence, as shown by curve 1. The circles in Fig. 4 fall between curve 1 and curve 2, indicating that some contribution from tail-state filling is present even at high pump powers. An intermediate case, where the two effects almost cancel each other, leading to a largely temperature-independent peak position, is shown by open squares in Fig. 4 (pumping rate of 15 W/cm^2). As the temperature rises from 10 to 300 K, the spectral bandwidth of InGaN emission increases slowly from ~46 meV to ~70 meV.

We have inspected the low-temperature behavior (at 11 K) in more detail and found that the pumping rate influences the peak position in accordance with the concept of degenerate occupation. With increasing pumping rate, the peak position marked by dots in Fig. 5 shifts continuously to higher photon energies by 26 meV. This behavior is qualitatively the same as that illustrated in Fig. 1a. Therefore, at low temperatures the spectral peak is rather sensitive to the pumping rate. At low pumping rates, the first type (non-monotonic) of behavior is observed; it converts into the second type (monotonic) at high pumping rates. Such evolution had been also observed in InGaN/ AlGaN/ GaN SQW LED electroluminescence spectra.[9–11,18,19]

In Fig. 6, we show a comparison of spectral peak position curves for GaN and InGaN emissions from a single sample (a SQW with an InGaN well layer thickness of 0.8 nm). A third type of behavior is observed for GaN (full dots), following closely the Varshni-like temperature dependence of Eq. 14. The corresponding fit 1 was obtained using $E_0(0)$ = 3.488 eV, α = 0.6 meV/K, and β = 700 K, which are quite reasonable for GaN. At low temperatures, the peak position is not very sensitive to the pumping rate, suggesting there is no substantial tailing. The low-temperature emission in undoped GaN is associated with excitons localized at point centers rather than with band-tails. The red shift of the PL emission peak from low temperatures to 300 K is ~55 meV, much more than in samples with band tails.

In contrast to the GaN emission spectra, the InGaN emission from the same sample is of the first type, namely, with some blue shift by a few meV in the middle-temperature range (100–150 K). The peaks at 30 K and at 250 K are at the same photon energy of ~3.16 eV, in sharp contrast to the Varshni-like behavior. Above 110 K, the experimental points are fitted by a "non-degenerate" curve 2 with tail parameter σ =

24 meV, $E_0(0) = 3.229$ eV, and $\alpha = 0.6$ meV/K. The value of β was taken here as 700 K, the same as in GaN. Note that fitting accuracy in β is rather poor, as it influences the temperature dependence in a rather weak fashion.

Perhaps the most important result of this study is that all homoepitaxial samples displayed Varshni-like behavior (see Fig. 7), indicating that homogeneity of these samples may be much better than in samples grown on sapphire. However, luminescence efficiency of the homoepitaxial samples is not high, which may well in fact be related to their improved homogeneity. Consequently, it is difficult to follow the InGaN-related peak above ~200 K. Instead of a clear maximum, some broad emission is observed at room temperature with multiple weak peaks. Low luminescence efficiency suggests that the actual excitation level (i.e., steady-state carrier concentration at any given level of pump power) is probably rather low even at low temperatures due to enhanced nonradiative recombination. The same conclusion can also be reached by integrating the spectra originating from the InGaN and GaN layers in the same samples. In addition, since the density of states in the bands is much higher than that in the tails, the temperature dependence of the spectral peak position is not influenced by the pumping rate as it was in the first two types of behavior. In summary, no evidence of band tailing was found in the homoepitaxial samples, in spite of their broad emission bandwidth (~62 meV at low temperatures).

Improved homogeneity of InGaN in homoepitaxial samples correlates with reduced threading dislocation density in those samples. This points out that threading dislocations are likely to act as preferred sites for In deposition during growth, leading to In-rich clusters around the dislocations. This interpretation is further supported by direct observation of cathodoluminescence (CL) in MOCVD-grown InGaN-GaN quantum wells on sapphire, correlated with AFM imaging.[22]

DISCUSSION

Effect of Carrier Capture to Band-Tail States on Radiative Recombination Efficiency

Excess carriers are more likely to recombine radiatively when captured into indium-rich clusters. Otherwise, they can diffuse to dislocations and other nonradiative sinks, and this is the most plausible explanation of poor radiative recombination efficiency of GaN and homoepitaxial InGaN. Observation of cathodoluminescence dark spots correlated with the TEM pattern of dislocations in GaN strongly indicates that threading dislocations can act as nonradiative recombination centers.[25] The hole diffusion length was estimated from that observation as ~50 nm at room temperature. If the capture into band-tail states shortens the diffusion length (below the average distance between dislocations), the band-tail recombination can restrict the nonradiative process at dislocations and on other extended defects. In

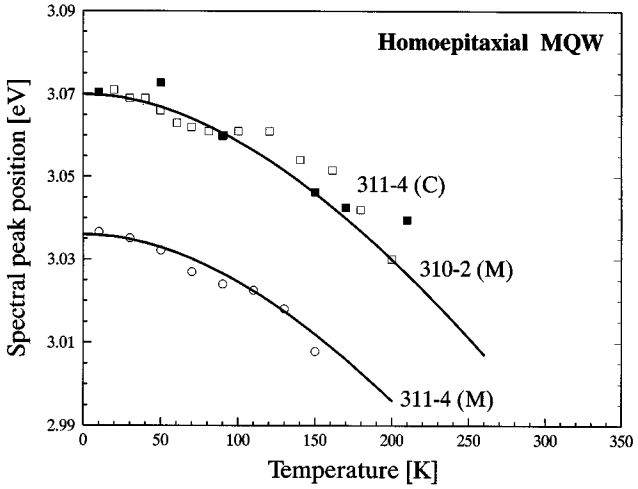

Fig. 7. PL peak position in function of temperature in homoepitaxial GaN/InGaN/GaN MQWs emitting in violet range (10 quantum wells, each 2-nm thick, separated by 5-nm-thick GaN barriers). C in brackets indicates a structure grown on the c-plane of GaN, M indicates a structure grown on m-plane of GaN. Experimental points are fitted using the Varshni expression (14).

a simple approach, the radiative quantum yield η can be expressed as follows:

$$\eta = 1 - (r_0/a)^2 - (2/a^2)\int_{r_0}^{a} \exp[-(r - r_0)/L_D]\, r\, dr$$
$$= 1 - (r_0/a)^2 - (2L_D/a^2)\{r_0 + L_D - (a + L_D)\exp[-(a - r_0)/L_D]\} \quad (16)$$

where r is the radial distance to the dislocation axis, r_0 is the radius of "dead zone" near the dislocation, $a = 1/2N_d^{-1/2}$ is the average half-distance between dislocations, and L_D is the ambipolar diffusion length of carriers. Reported values of hole diffusion length L_p for GaN range from 50 nm[25] to an estimated upper limit of 250 nm,[26] while r_0 was estimated to be 50 nm by observation of CL dark spots associated with threading dislocations.[25] At $N_d = 10^8$ cm^{-2}, Eq. 16 gives $\eta \approx 95\%$ at $L_D = 50$ nm and $\eta \approx 79\%$ at $L_D = 150$ nm. At $N_d = 10^9$ cm^{-2}, the radiative efficiency falls to $\eta \approx 60\%$ at $L_D = 50$ nm and $\eta \approx 30\%$ at $L_D = 150$ nm. Therefore, the quantum yield can be of device quality in spite of the high dislocation density and high nonradiative recombination efficiency of dislocations, but will drop rapidly when N_d exceeds 10^8 cm^{-2}.

It is not usual in optoelectronic semiconductors that a smaller diffusion length of excess carriers could lead to a higher radiative quantum yield. However, in the framework of this approach, Eq. 16 predicts higher η if the diffusive transport of excess carriers to dislocations is reduced by trapping of carriers into tail states. This can be an important factor influencing the excellent light-emission performance of InGaN with In content corresponding to blue and green light emission. Other defects and nonradiative centers can limit the positive effect of capture by the tail states in materials with high average In content, approaching the yellow light emission range.

Table I. Band-Tail Parameters in GaN and InGaN Epitaxial Structures*

Structure	Method	x [%]	ΔE [meV]	$E_0(0)$ [eV]	σ [meV]
GaN, thick (~1 μm) epilayer	PL	0	~0	~3.48	< 2
InGaN, DH, d = 40 nm[a]	PL	2	~3	3.432	8
InGaN:Si, SH[b]	PL	6	6	3.387	13.7
InGaN, MQW[c]	PL	~20	7.6	~3.4	6.5
InGaN, SH, d = 110 nm	PL	8.5 ± 1.5	20	3.34	10
InGaN, DH, d = 40 nm	PL	7.5 ± 1.5	30	3.284	14
InGaN, SH, d = 200 nm[d]	PL	20	24	3.05	16
InGaN, SQW, d = 1.4 nm	PL	~20	17	2.862	18
InGaN, SQW, d = 2.5 nm[e]	EL	15 – 30	52	2.78	31.5
InGaN, SQW, d = 2.5 nm[e]	EL	30 – 45	30	2.394	28.6
InGaN, SQW, d = 2.5 nm[e]	EL	30 – 45	59	2.392	35
InGaN, MQW, d = 10 × 2 nm (homoepitaxial)	PL	~20	0	3.036	~0

*ΔE is the temperature-induced blue spectral shift; $E_0(0)$ and σ are fitting parameters.
[a] Derived from PL spectral peak position plot.[27]
[b] Derived from PL measurements.[28]
[c] PL study reported in Ref. 29. Peak near 3.4 eV suggests lower x than 20% indicated in Ref. 29.
[d] Derived from experimental plots.[30]
[e] Electroluminescence (EL) study reported in Ref. 11.

Experimental Determination of σ Parameter

In the previous section, we fit the experimental curves for the PL peak position vs. temperature using Eqs. 13 and 14. The same procedure can also be applied to other published data where a blue temperature-induced shift can be identified. The fitting results are summarized in Table I. It is clear that pronounced tailing is characteristic of InGaN alloys, but not of GaN (at least in undoped samples). The tail parameter σ correlates with an average indium content and increases from about zero in GaN to 30–35 meV in green-light-emitting structures. The tailing is found in both thick epilayers and in QWs on sapphire, but not in homoepitaxial samples on sublimation-grown GaN substrates.

Consider now the tail parameter σ from the point of view of microscopic material properties. Our first hypothesis is that the tail states are not quantum-confined states, due to slow variation of the band edges. The effect can therefore be treated in the framework of tilted-band-edge approximation, used in the above calculation of the DOS distribution. Deeper tail states are associated with clusters of larger indium molar fraction x. The magnitude of σ characterizes the energy scale for a substantial decrease in DOS. Using the average value of $dE_g/dx \approx -2$ eV in the range about x = 0.20, the composition variation corresponding to σ = 30 meV can be estimated to be ~0.015, which is quite plausible.

In the case of QWs, the variation of quantum-confined levels could in principle also be associated with fluctuations of the well thickness L_z. Using the infinite well approximation, sensitivity of the photon energy to QW thickness variation can be expressed as

$$d(h\nu)/dL_z \approx -\pi^2\hbar^2/(m_{red}L_z^3) \qquad (17)$$

where m_{red} is the reduced effective mass. When the average value of L_z is 3 nm, a change in the photon energy by 30 meV can result from a local increase in L_z to 5 nm. However, deep states inside the tail (3–5 times σ below nominal bandgap) would require an unreasonably high increase in the well thickness and may not even be attainable, since the bulk nominal bandgap represents the ultimate limit of well-thickness-related shift in energy level. In addition, the thickness variation interpretation could not be applied at all to a bulk material. We therefore conclude that In content variations are a much more likely cause of the band tail states than the well thickness fluctuations.

Another hypothesis is that the tail states are quantum-confined states. We restrict the consideration to a particular case when the random variation in the lateral well size determines the dispersion of the energy level position in QWs, whereas variations of the well depth are minimal (see Appendix). We use Eq. A3 in order to estimate the average lateral size of random wells. We assume the following numerical parameters: well depths $U_{0e} = U_{0h} = U_0 = 0.5$ eV, $m_e = 0.18\ m_0$, $m_h = 0.8\ m_0$, σ = 30 meV, and a large relative variation of size, $\sigma_R/R_0 \approx 1$. With these assumptions, we have an expression

$$R_0 = (\hbar/\sigma)(\sigma_R/R_0)(2U_0/m_{red})^{1/2} = 24 \text{ nm} \qquad (18)$$

This estimate looks reasonable, and such clusters are rather large. Considering the total number of In atoms in such a cluster, statistical fluctuations of indium composition can produce deviations not higher than 0.5% from the average composition of x = 0.20. Therefore, composition variations are not of purely statistical nature, but result from some segregation process. For example, presence of threading dislocations during growth can result in local enhancement of In content.[22]

CONCLUSIONS

Photoluminescence (PL) of InGaN/GaN bulk and quantum-well (QW) structures has been investigated

and interpreted in terms of band-tail luminescence typical for structures grown on sapphire substrates. Different types of temperature dependence of the spectral peak position are identified. In the case of pronounced band-tailing, the dependence departs significantly from the usual Varshni-like bandgap shift. The PL peak is red-shifted with respect to the nominal bandgap energy, similarly to the Stokes shift. The tail-induced shift depends on temperature in a simple manner, producing an anomalous blue shift of the spectral peak with increasing temperature. Such shifts were observed in electroluminescence spectra of InGaN QWs[9–11,18,19] and later reported in other studies of both electroluminescence and photoluminescence in InGaN. The anomalous temperature-induced blue shift of the peak position can be used to estimate the tail parameter σ that describes the density-of-states distribution in the tails. The σ parameter correlates with the average indium content in the alloy. The tailing effect is associated with alloy composition variations observed in both QW and bulk epilayers. Threading dislocations are a likely factor enhancing compositional inhomogeneities in InGaN. On the other hand, in homoepitaxial material (QW structures on sublimation-grown bulk GaN substrates) and in undoped GaN epilayers, the temperature anomaly is not observed and σ is estimated to be near zero.

From the above discussion concerning the band-tail model and its comparison with experimental data, we can conclude the following:

1) There is a clear semi-quantitative agreement between the predicted effect of band tails on the spectral behavior of InGaN emission and the experimental PL data from InGaN-based epitaxial structures grown on sapphire substrates. The characteristic blue temperature-induced shift of the peak position was observed in all samples, including thick epilayers (50–110 nm) and different QW structures (with well thicknesses as small as 0.8 nm). This phenomenon is associated with band-tail formation due to compositional variations of the alloy, assisted by the presence of numerous dislocations.
2) The tail parameter σ is derived from the temperature dependence of the peak position and is found to correlate with the average indium content in the InGaN alloy. This parameter is practically zero in undoped GaN and grows to 30–40 meV in green-light-emitting InGaN structures. The σ parameter is suggested to describe the inhomogeneous broadening of the band edges due to bandgap variations in the alloy.
3) In sharp contrast to InGaN samples grown on sapphire, there is no evidence for band tailing in homoepitaxial structures grown on bulk GaN needles as substrates. The PL efficiency in these structures is found to be rather low, indicating much stronger nonradiative recombination. We interpret this as evidence that the capture of carriers into tail states is favorable to radiative processes, preventing the diffusion of excess carriers to extended defects (dislocations, etc.).

ACKNOWLEDGEMENTS

This work was supported by DARPA under the Optoelectronic Materials Center program and by AFOSR. One of the authors (PGE) expresses his gratitude to the University of Tokushima for a possibility to stay there and to join the nitride studies at Satellite Venture Business Laboratory during December 1998–February 1999. The authors are thankful to Vladimir A. Smagley of the University of New Mexico for his assistance in some of the calculations reported in this paper.

REFERENCES

1. S.N. Mohammad and H. Morkoç, *Prog. Quantum Electron*. 20, 361 (1996).
2. S. Nakamura and G. Fasol, *The Blue Laser Diode: GaN Based Light Emitters and Lasers* (Berlin: Springer-Verlag, 1997).
3. J.W. Orton and C.T. Foxon, *Rep. Prog. Phys.* 61, 1 (1998).
4. O. Ambacher, *J. Phys. D: Appl. Phys*. 31, 2653 (1998).
5. I.V. Akimova, P.G. Eliseev, and M. Osinski, *Quantum Electron*. 28, 987 (1998).
6. S. Chichibu, T. Azuhata, T. Sota, and S. Nakamura, *Appl. Phys. Lett.* 69, 4188 (1996).
7. Y. Narukawa, Y. Kawakami, M. Funato, S. Fujita, S. Fujita, and S. Nakamura, *Appl. Phys. Lett.* 70, 981 (1997).
8. I.V. Akimova, P.G. Eliseev, M.A. Osinski, and P. Perlin, *Quantum Electron.* 26, 1039 (1996).
9. M. Osi**n**ski, P. Perlin, P.G. Eliseev, and J. Furioli, *Light-Emitting Diodes: Research, Manufacturing, and Applications*, *SPIE Proc. 3002,* ed. E.F. Schubert (Bellingham, WA: SPIE, 1997), p. 15.
10. P. Perlin, M. Osinski, and P.G. Eliseev, *III-V Nitrides*, ed. F.A. Ponce, T.D. Moustakas, I. Akasaki, and B.A. Monemar (Pittsburgh, PA: Mater. Res. Soc., 1997), p. 1173.
11. P.G. Eliseev, P. Perlin, J. Lee, and M. Osinski, *Appl. Phys. Lett*. 71, 569 (1997).
12. K.G. Zolina, V.E. Kudryashov, A.N. Turkin, and A.E. Yunovich, *MRS Internet J. Nitride Semicond. Res.* 1, Art. 11 (1996).
13. H.C. Casey, Jr., J. Muth, S. Krishnankutty, and J.M. Zavada, *Appl. Phys. Lett.* 68, 2867 (1996).
14. E.O. Kane, *Solid-State Electron*. 28, 3 (1985).
15. P.G. Eliseev, M.A. Manko, A.I. Krasilnikov, and I.Z. Pinsker, *Phys. Stat. Sol.* 23, 587 (1968).
16. L. Robins, A.J. Paul, C.A. Parker, J.C. Roberts, S.M. Bedair, E.L. Piner, and N.A. El-Masry, *MRS Internet J. Nitride Semicond. Res.* 4S1, Article G3.22 (1999).
17. B.D. Little, W. Shan, J.J. Song, Z.C. Feng, M. Schurman, and R.A. Stall, *III-V Nitrides*, ed. F.A. Ponce, T.D. Moustakas, I. Akasaki, and B. A. Monemar (Pittsburgh, PA: Mater. Res. Soc., 1997), p. 823.
18. M. Osinski, P.G. Eliseev, P. Perlin, V.A. Smagley, J. Furioli, and J.-H. Lee, *Record of the 16th Electron. Mater. Symp*. (Osaka, Japan: 1997), p. 273.
19. M. Osinski P. Perlin, P.G. Eliseev, J. Lee, and V.A. Smagley, *Nitride Semiconductors 1997, Proc. of the 2nd International Conf. on Nitride Semiconductors*, ed. K. Hiramatsu, K. Kishino, S. Nakamura, and H. Amano, *Special Issue J. Cryst. Growth* 189/190 (Amsterdam: North-Holland, 1998), p. 803.
20. S. Sakai, H. Sato, T. Sugahara, Y. Naoi, S. Kurai, K. Yamashita, S. Tottori, M. Hao, and K. Nishino, *Mater. Science Forum* 264, 1107 (1998).
21. H. Sato, T. Sugahara, Y. Naoi, and S. Sakai, *Jpn. J. Appl. Phys., Pt. 1* 37, 2013 (1998).
22. T. Sugahara, M. Hao, T. Wang, D. Nakagawa, Y. Naoi, K. Nishino, and S. Sakai, *Jpn. J. Appl. Phys., Pt. 2 (Lett.)* 37,

L1195 (1998).
23. T. Wang, D. Nakagawa, M. Lachab, T. Sugahara, and S. Sakai, *Appl. Phys. Lett*. 74, 3128 (1999).
24. S. Sakai, *J. Korean Phys. Soc.* 34, S220 (1999).
25. T. Sugahara, H. Sato, M. Hao, Y. Naoi, S. Kurai, S. Tottori, K. Yanashita, K. Nishino, L. Romano, and S. Sakai, *Jpn. J. Appl. Phys*., *Pt. 2 (Lett.)* 37, L398 (1998).
26. S.J. Rosner, E.C. Carr, M.J. Ludowise, G. Girolami, and H.I. Erikson, *Appl. Phys. Lett*. 70, 420 (1997).
27. Y. Narukawa, S. Saijou, Y. Kawakami, S. Fujita, T. Mukai, and S. Nakamura, *Appl. Phys. Lett.* 74, 558 (1999).
28. T. Taguchi, T. Maeda, Y. Yamada, S. Nakamura, and G. Shinomiya, *Blue Laser and Light Emitting Diodes*, ed. A. Yoshikawa, K. Kishino, M. Kobayashi, and T. Yasuda (Tokyo, Japan: Ohmsa, Ltd., 1996), p. 372.
29. K.L. Teo, J.S. Colton, P.Y. Yu, E.R. Weber, M.F. Li, W. Liu, K. Uchida, H. Tokunaga, N. Akutsu, and K. Matsumoto, *Appl. Phys. Lett*. 73, 1697 (1998).
30. S. Chichibu, L. Sugiura, J. Nishio, A. Setoguchi, H. Nakanishi, and K. Itaya, *Blue Laser and Light Emitting Diodes*, ed. K. Onabe, K. Hiramatsu, K. Itaya, and Y. Nakano (Tokyo, Japan: Ohmsa, Ltd., 1998), p. 616.

APPENDIX. TAIL PARAMETER σ IN THE CASE OF SIZE VARIATION

Consider the value of σ in the particular case of tail formation where the depth of wells is nearly constant, but their size can vary considerably. We use the model of the "quantum disk" for the indium-rich clusters with a parabolic shape of the potential energy profile. The bottom of all wells is assumed to be at the same energy, whereas the energy of the quantum-confined level E_{loc} (the kinetic energy of localization, calculated from the bottom of the well) varies depending on the well size. For a parabolic well, the energy E_{loc} corresponds to the well known case of harmonic oscillator, and it depends on the oscillator mass and curvature of the potential energy profile. It is convenient to express it in terms of the well depth U_0 and the well radius R as follows

$$E_{loc} = (\hbar/R)(2U_0/m^*)^{1/2} \quad \text{(A1)}$$

where U_0 is the well depth and m* is effective mass of the captured carrier. We consider the dispersion of E_{loc} to represent the parameter σ^2 for each carrier type. For example, for electrons

$$\sigma_e^2 = 2\hbar^2 U_{0e}\sigma_R^2/(R_0^4 m_e) \quad \text{(A2)}$$

where σ_R^2 is the dispersion of the well radius, R_0 is its average value, U_{0e} is the electron well depth, and m_e is the effective mass of electrons. Analogous expression can be written for holes with well depth U_{0h} and the mass m_h. By adding dispersions for both types of carriers, we obtain the total tail parameter

$$\sigma = (2^{1/2}\hbar/R_0)(\sigma_R/R_0)[(U_{0e}/m_e) + (U_{0h}/m_h)]^{1/2} \quad \text{(A3)}$$